ISSN 0001-4338, Izvestiya, Atmospheric and Oceanic Physics, 2012, Vol. 48, No. 7, pp. 706–716. © Pleiades Publishing, Ltd., 2012.
Original Russian Text © V.A. Ozheredov, T.K. Breus, V.N. Obridko, 2011, published in Geofizicheskie Protsessy i Biosfera, 2011, No. 3, pp. 51–65.

Prediction of the Total Cycle 24 of Solar Activity by Several Autoregressive Methods and by the Precursor Method

V. A. Ozheredov[a], T. K. Breus[a], and V. N. Obridko[b]

[a] *Space Research Institute, Russian Academy of Sciences, Profsoyuznaya ul. 84/32, Moscow, 117997 Russia*
e-mail: ojymail@mail.ru; breus36@mail.ru

[b] *Institute of Terrestrial Magnetism, the Ionosphere, and Radio-Wave Propagation, Russian Academy of Sciences, Troitsk, Moscow oblast, 142190 Russia*
e-mail: obridko@mail.ru

Abstract—As follows from the statement of the Third Official Solar Cycle 24 Prediction Panel created by the National Aeronautics and Space Administration (NASA), the National Oceanic and Atmospheric Administration (NOAA), and the International Space Environment Service (ISES) based on the results of an analysis of many solar cycle 24 predictions, there has been no consensus on the amplitude and time of the maximum. There are two different scenarios: 90 units and August 2012 or 140 units and October 2011. The aim of our study is to revise the solar cycle 24 predictions by a comparative analysis of data obtained by three different methods: the singular spectral method, the nonlinear neural-based method, and the precursor method. As a precursor for solar cycle 24, we used the dynamics of the solar magnetic fields forming solar spots with Wolf numbers *Rz*. According to the prediction on the basis of the neural-based approach, it was established that the maximum of solar cycle 24 is expected to be 70. The precursor method predicted 50 units for the amplitude and April of 2012 for the time of the maximum. In view of the fact that the data used in the precursor method were averaged over 4.4 years, the amplitude of the maximum can be 20–30% larger (i.e., around 60–70 units), which is close to the values predicted by the neural-based method. The protracted minimum of solar cycle 23 and predicted low values of the maximum of solar cycle 24 are reminiscent of the historical Dalton minimum.

Keywords: Wolf numbers, solar cycle 24 predictions, autoregressive methods, neural-based approach, precursor method.

DOI: 10.1134/S0001433812070043

1. INTRODUCTION

1.1. Overview of Approaches to Solar Cycle Prediction

The prediction of solar activity over the next few years and a forecast of the characteristics of the next cycle are among the oldest problems in solar physics. However, we cannot say that in recent years they have been successfully resolved.

In general, methods for predicting solar cycles can be conditionally divided into two types. The first type includes methods of statistical extrapolation (or autoregressive methods), when the analysis involves a single time series to be properly predicted. The horizon of prediction of the *Rz*-index by autoregressive methods is normally several months or years.

Most researchers involved in the forecast of solar activity have used these methods. This type of study refers to a significant portion of existing predictions ranging from classical works [*McNish and Lincoln*, 1949; *Obridko*, 1996] to the present time [*Cane*, 2001, 2002; *Loskutov et al.*, 2001], including studies that are based on neural networks as well [*McPherson et al.*, 1995; *Fessant and Lantos*, 1996].

The second type of predictions, which is called the precursor method, uses additionally one or more time series, such as third-party helio-geophysical data [*A.I. Ohl and G.I. Ohl*, 1979; *Feynman*, 1982; *Thompson*, 1993; *Hathaway et al.*, 1999 ; *Lantos and Richard*, 1998]. In some cases, the precursor methods improve the prediction because they are based on some kind of physical model.

1.2. The State of the Problem of Predicting Cycle 24

Solar cycle 24 is characterized by considerable scatter in the predicted values of the maximum. According to the statement of the Third Official Solar Cycle 24 Prediction Panel created by the National Aeronautics and Space Administration (NASA), the National Oceanic and Atmospheric Administration (NOAA), and the International Space Environment Service (ISES), which is based on the results of an analysis of many solar cycle 24 predictions by different

methods, there are two possible scenarios for the amplitude and time of the maximum: 90 units and August 2012 or 140 units and October 2011, respectively [*Makarov and Tlatov*, 2000; *Schatten*, 2002, 2003; *Wang et al.*, 2002; *Duhau*, 2003; *Meyer*, 2003; *Svalgard et al.*, 2005; *Douglas and Biesecker*, 2008; etc.].

From these data, it is evident that the prediction of solar cycle 24 is still relevant. Recently, a number studies have been published with an analysis and criticism of the earlier used methods [*Petrovay*, 2010], as well as a discussion of the situation in the interplanetary space and the behavior of the near-Earth space characteristics pointing to extremely low values of all parameters on the descending branch of cycle 23 and implying a scenario for solar activity in the next cycles resembling the historical Dalton minimum [*Russell et al.*, 2010].

This paper attempts to predict solar cycle 24 by different methods, which makes it possible to compare their advantages and limitations and choose an optimal prediction scenario.

2. DIFFERENT APPROACHES TO THE PREDICTION OF SOLAR CYCLE 24 USED IN THIS STUDY

2.1. Linear and Singular Spectral Predictions

In this paper we used a series of daily data on variations of *Rz* in cycles 21, 22, and 23 of solar activity (January 6, 1977 to November 30, 2010) taken from the website www.noaa.gov. We used autoregressive methods dealing with a single time series *Rz* and predicting its extension. To this end, the original time series is divided into realizations (Fig. 1a) consisting of predictors that form lags (i.e., those readings that expectedly affect the subsequent readings of the series) and adaptors (i.e., those subsequent readings that will be predicted in the course of learning of the algorithm). Then, the algorithm learns to predict these existing adaptors, i.e., reveals the dependence of adaptors on predictors using some part of the series (a learning sequence of readings). The algorithm identifies the dependence between the values k of terminal readings of realizations (Fig. 1a) and predictors on the learning interval W (identifying these predictors and adaptors) for the time series under investigation. The dependence between each of the k terminal readings of the implementation and the lag is assumed to be linear. Geometrically, it is a Q-dimensional hyperplane. Figures 1b–1d show a two-dimensional hyperplane as an example. In the case of iterative prediction, we have $k = 1$; i.e., the prediction covers a single reading of the given series. In the case of noniterative prediction, we have $k > 1$; i.e., the adaptor is represented here by a vector and the prediction covers several readings forward (Fig. 1a). The set of predictors that are followed by the predicted readings is called forward lag. The search for a hyperplane is carried out by singular spectral analysis (SSA).

SSA makes it possible to predict the spectral components of time series that are least exposed to the influence of noise.

Unlike the autoregressive linear prediction, the regular spectral prediction is characterized by the fact that only individual spectral components of time series are predicted. In this case, the spectral basis is usually specified a priori (see, for example [*McNish and Lincoln*, 1949; *Cane*, 2001, 2002]). The singular spectral prediction optimizes the basis to identify a subspace that is least affected by noise. Each realization of the time series is projected onto this special basis, in which a subspace of directions with a minimum variance is chosen. It is assumed that the noise variance is the same for all directions, while the directions with a maximum variance (i.e., part of the spectral components of the series) will have a highest signal-to-noise ratio [*Pyt'ev*, 1990; *Ozheredov et al.*, 2009]. Normally, this makes the prediction smooth, since there are no unreliable variations.

Figure 2a (right) shows the dependence of the error (see the scale) on the dimension of hyperplane Q and the size W of the learning interval. The error is the sum of squared differences of predicted and actual values of the series and it reaches a minimum (deep blue color) in the case of a successful prediction. As can be seen from Fig. 2, there are several such areas. Due to this, the seemingly successful predictions of individual cycles of solar activity (Figs. 2a, 2b) would make it possible in each case to pick up pairs of adequate values of Q and W. However, one does not manage to make a prediction using the same values of these parameters for the entire series of given cycles (Figs. 2, 3), which means that there is no general regularity for the formation of the entire series of cycles and the prediction of solar cycle 24 by this method becomes uncertain.

The iterative prediction (see Figs. 2, 3) has the specific feature of accumulating a significant amount of errors as the horizon of forecast increases; this method is mainly suitable for short-term forecasts (Fig. 3b).

The noniterative prediction allows for the prediction of long-term variations of time series, for example, two cycles (22 and 23), as is shown in Fig. 4a. However, this prediction is insufficiently adaptive. This leads to a mismatch between predicted and actual variations in Wolf numbers *Rz* (see the rise in the predicted branch of *Rz* at the end of cycle 23 in Fig. 4a) and a mismatch between cycles 23 and 24 in Fig. 4b for the prediction of cycle 24 and part of cycle 25.

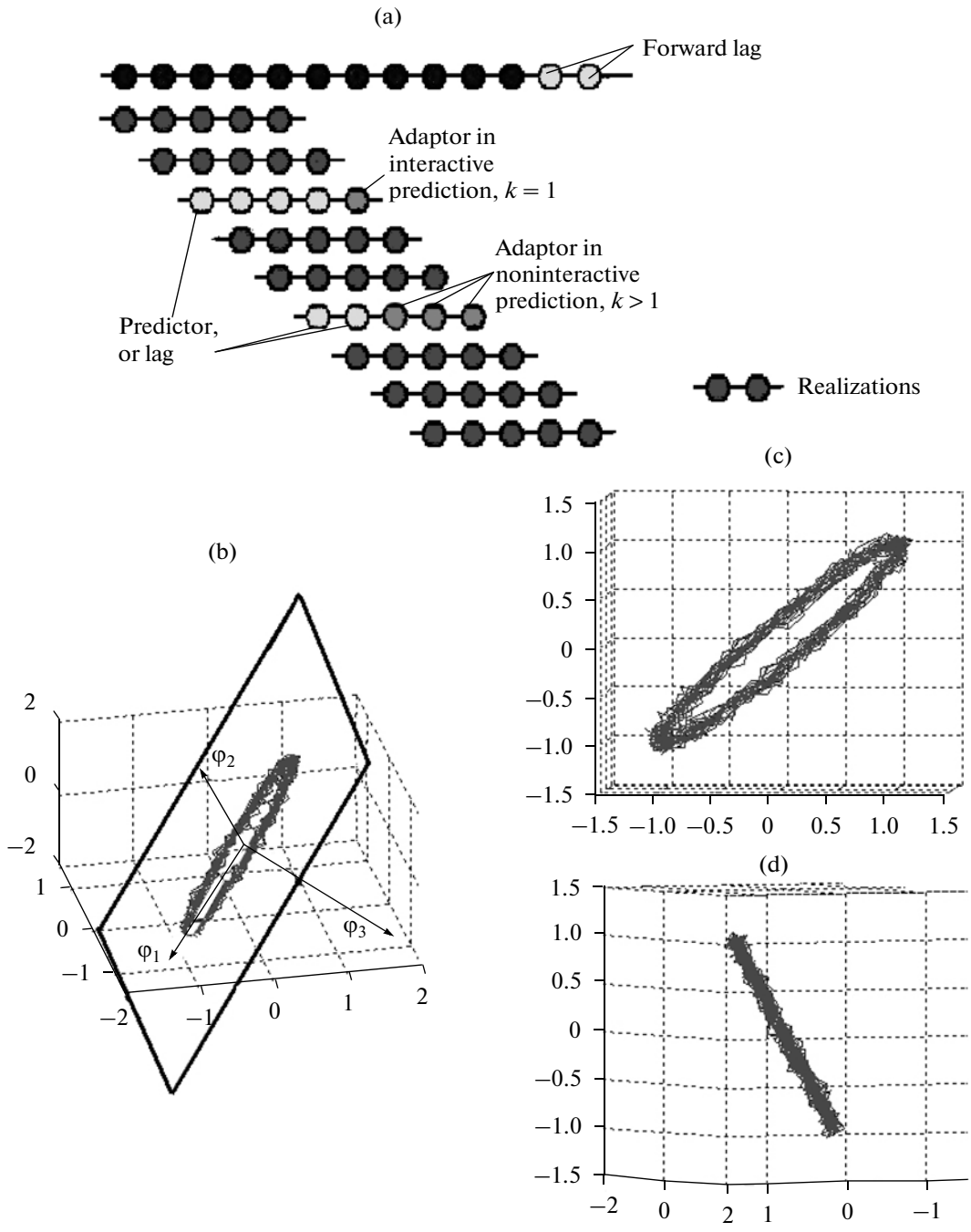

Fig. 1. Schematic of the formation of predictions: (a) separation of the original time series into realizations; (b) the behavior of the realization vector in the space for the case of a three-dimensional realization vector. The remaining explanations are given in the text.

2.2. Iterative Nonlinear Prediction of Cycle 24 by the Neural-Based Approach

In the iterative prediction using the neural-based approach (in a multidimensional space of lag vectors) when the dependence of adaptors on predictors in principle is nonlinear, one can assume that the dependence is linear in some neighborhood of the forward lag (see Fig. 1a). The main problem is the search for this neighborhood or, essentially the same thing, precedents of it: the nearest neighbors to this forward lag. The search for the nearest neighbors (in our case, in a 75-dimensional space of lag vectors) was conducted using the Neurons with Adaptive Turn of Restricting Ellipsoid (NATRE) special-purpose neural network,

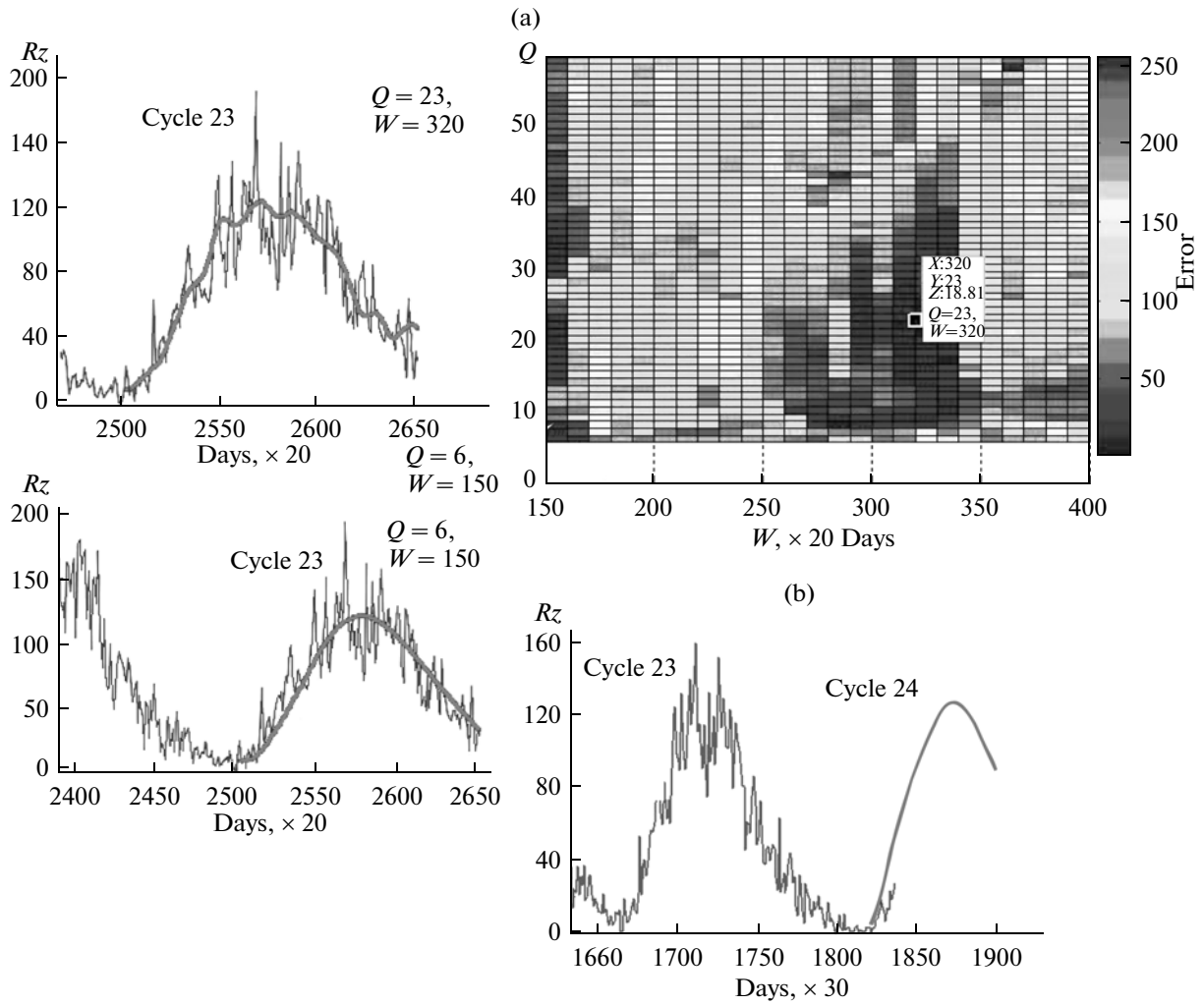

Fig. 2. Examples of prediction (red line) of (a) cycle 23 and (b) cycle 24 (b) by the iterative prediction method. Time is given in 20- and 30-day intervals.

where the nearest neighbors are determined in conformity with the Mahalanobis optimal distance[1] [*Mahalanobis*, 1936].

As can be seen in Fig. 5a, this forecast, made for all the initial cycles, including the cycle 22, gives a rather satisfactory prediction of solar cycle 23 with a protracted descending branch. The good agreement between the original and the prediction in cycle 23 allows us to hope that the forecast for cycle 24, made likewise for the entire original series of cycles, including cycle 23 (i.e., the entire time series of learning) with the same lag length (Fig. 5b), is reliable. It gives a good agreement between predicted and actual values of Wolf numbers *Rz* up to May 2011 and predicts a maximum of 70 units for cycle 24 (Fig. 5b).

Like in previous studies carried out on the basis of fundamentally different neural networks [*McPherson et al.*, 1995; *Fessant and Lantos*, 1996], the amplitude of the maximum of solar cycle 24 turned out to be around 145. The discrepancy with our result may be due to the fact that the abovementioned studies could not take into account cycle 23 and used data of a period before the onset of cycle 23. In view of this, to get a successful prediction of cycle 24, these studies had to use a forecast horizon covering two cycles (more than 20 years), which is a difficult task with the iterative prediction (as was shown above).

[1] The Mahalanobis distance (introduced by the Indian statistician P.C. Mahalanobis in 1936) is a measure of the distance between vectors of random variables, generalizing the concept of Euclidean distance. Using Mahalanobis distance, one can identify the *similarity* between unknown and known samples. It differs from Euclidean distance in that it takes into account the correlations between variables and is scale-invariant.

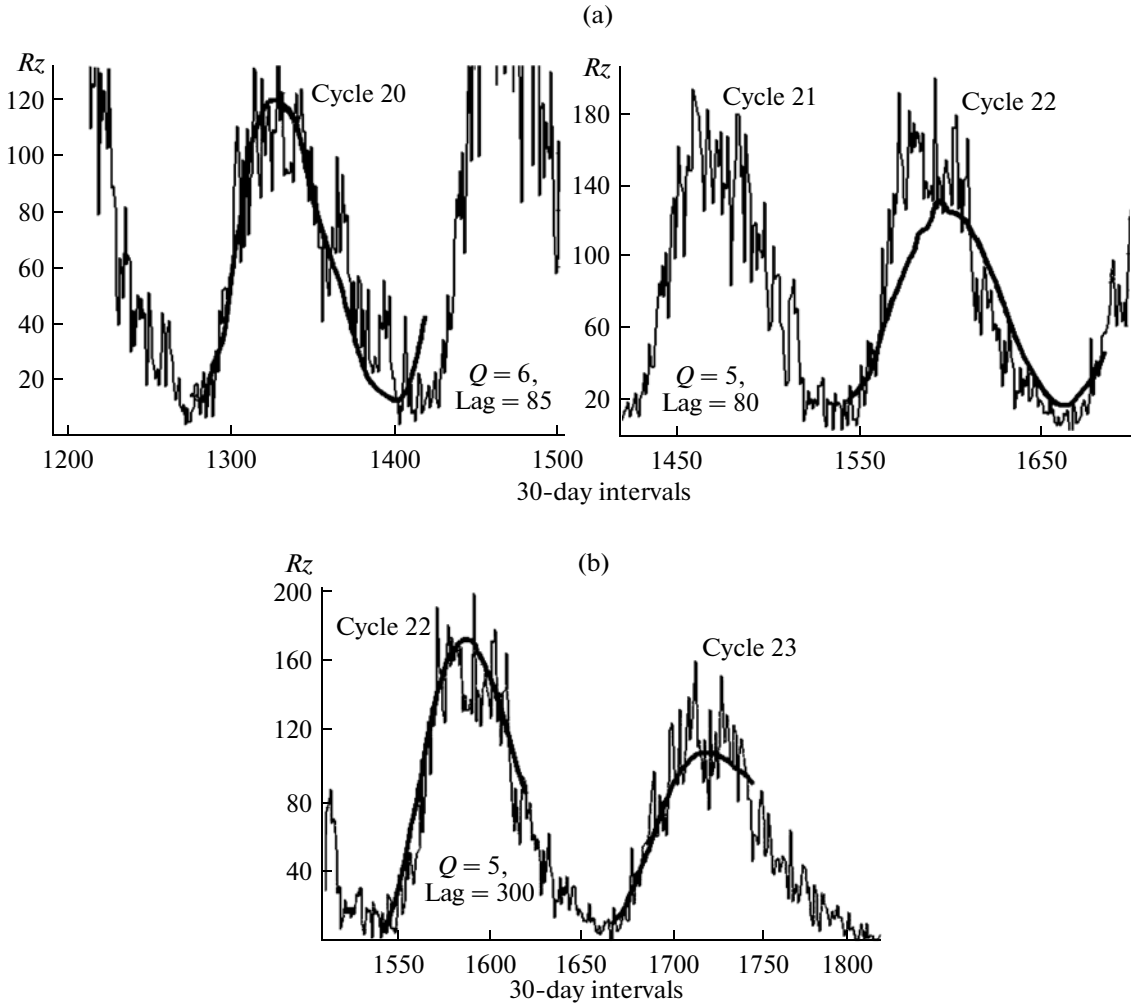

Fig. 3. Examples of iterative prediction (bold lines) of total cycles 20 and 22, indicating (a) a significant mismatch with actual data and (b) a successful simultaneous prediction of parts of cycles 22 and 23.

3. THE PRECURSOR METHOD

3.1. The Choice of Precursor

Next, we attempted to extend the horizon of the forecast of Wolf numbers *Rz* by using the precursor method, i.e., an independent time series with a leading series that correlates with the original series.

The precursor for predicting cycle 24 relies on the notion of dynamics of solar magnetic fields that generate sunspots, i.e., basis data to estimate the actual variations of Wolf numbers *Rz*.

At the first stage, according to the mechanism of generation of solar magnetic fields proposed by Parker (alpha–omega–dynamo), a poloidal magnetic field turns into a toroidal field due to solar rotation (the so-called omega effect). The index of the Sun's toroidal field is the equatorial magnetic field *ef*. The *Rz*-index reflects the variations of this field. The index of the poloidal field is the polar field *pf*. This process determines the generation of the solar cycle and characterizes its ascending branch with a length of 4—5 years.

At the second stage, the poloidal field is restored through the torsion and extension of the toroidal field (alpha effect). This part of the field dynamics corresponds to the descending part of the solar activity cycle, remaining controversial.

In our case, the *Rz*-series is appended as a predictor (in other words, independent variable) by the time series of the quadratic function of approximation of *Rz* modulo *pf*, i.e., $q(|pf|)$, which correlates with the *Rz*-series with a positive shift Δt. This series is represented by the square transformed magnitude of the polar field *pf*. If the horizon of the autoregressive prediction of *Rz* is T, then, when the predictor $q(|pf|)$ is strongly correlated with *Rz*, the horizon of autoregressive prediction of $q(|pf|)$ is also equal to T and, taking into account the

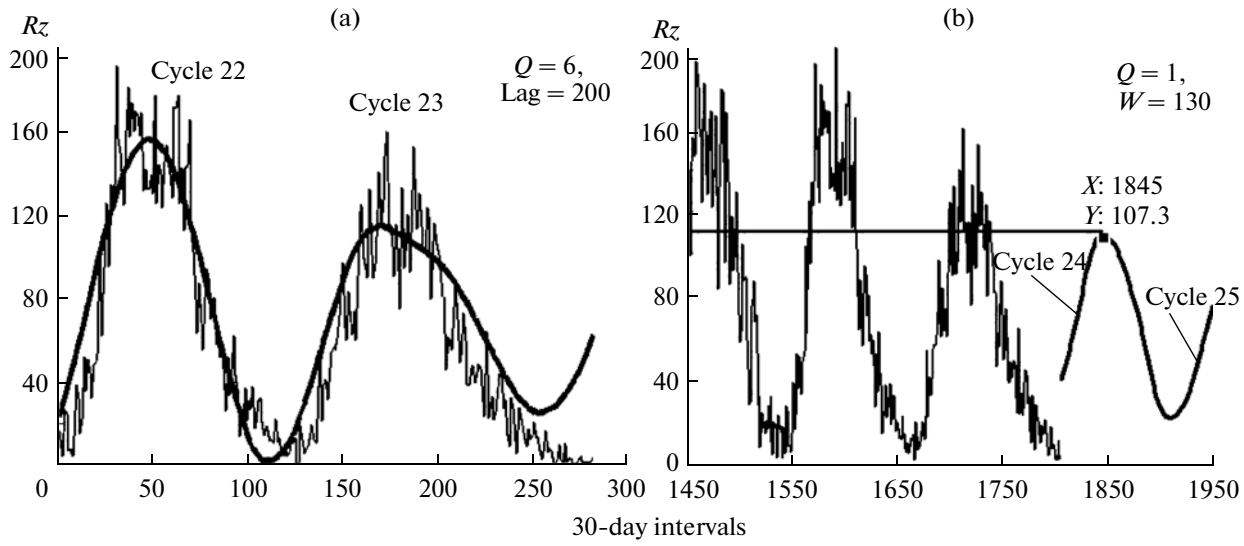

Fig. 4. Examples of a noniterative prediction of cycles 22, 23, and 24. Explanations are given in the text.

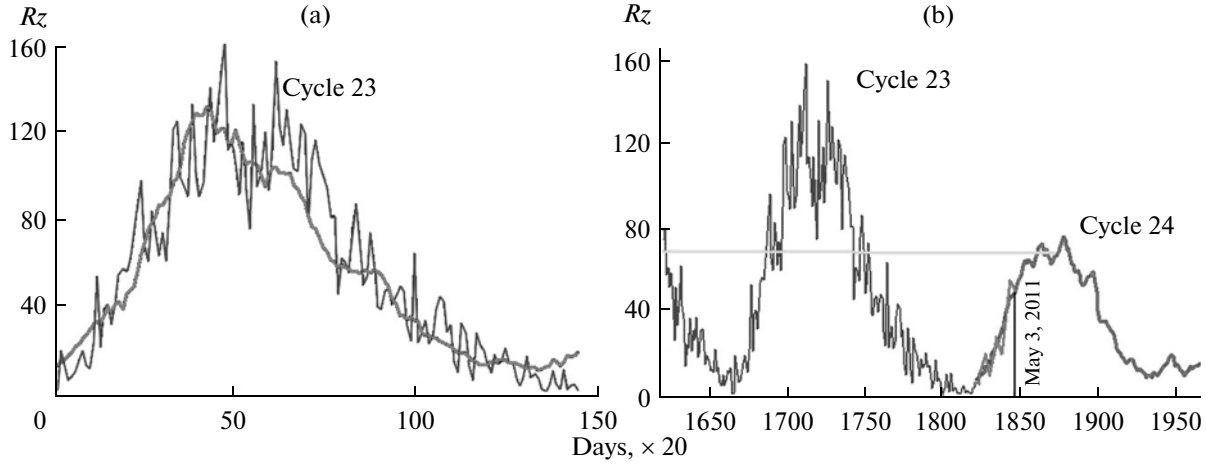

Fig. 5. Iterative prediction of cycles 23 and 24 using the neural-based approach. The blue curves (a) and (b) denote the actual values of *Rz* for cycle 23; the red curves in (a) and (b) denote the prediction of cycle 23 (a) and the actual readings of *Rz* of the initial phase of cycle 24 (b); the green curve in (b) denotes the prediction of cycle 24.

shift between the series, the effective horizon of the prediction of *Rz* becomes equal to $T + \Delta t$.

The variations in the predictor *pf* in solar cycle 24 were predicted using singular spectral analysis.

Figure 6 shows a series of measurement data on the polar field *pf* with a step of 10 days (see http://wso.stanford.edu/gifs/Polar.gif).

To reveal the significant variations of *Rz*, we used data on the equatorial field *ef* taken in the same interval of measurements as the polar field *pf* given at the same website.

3.2. Results of Analysis

To eliminate the noise in the *Rz* series, we performed an averaging operation. The interval of averaging was chosen on the basis of the coefficient of correlation between the values of *Rz* and *ef,* since it was assumed that the main large-scale variations of *Rz* repeat the variations of *ef*. Figure 7 shows the dependence of the correlation coefficient on the averaging interval.

The optimal interval was chosen so as to maximize the coefficient of correlation between the smoothed series of *Rz* and *ef*, provided that the averaging interval

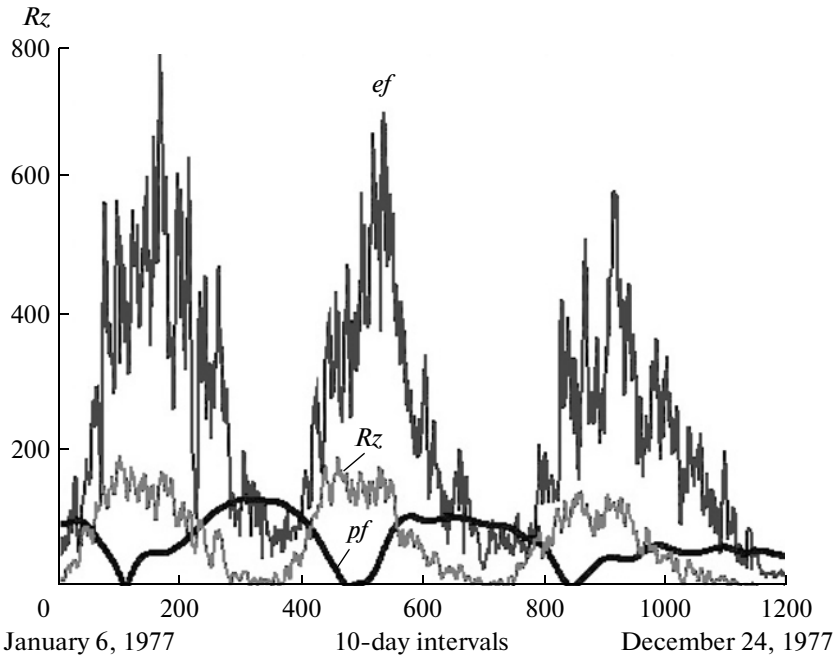

Fig. 6. Original data by *Rz*, *ef*, and modulo *pf*, taken with an interval of 10 days.

does not exceed values comparable with the 11-year cycle, i.e., when the 11-year periodicity may be lost. It can be seen from Fig. 7 that the optimal averaging period constitutes 160 10-day intervals (or $160 \times \frac{10}{365} =$ 4.4 years.

Figure 8 shows the results of averaging of *Rz*, *ef*, and the magnitude of the polar field *pf*.

Then, we search for the optimal precursor *ef* and the magnitude of *pf* with a shift, which will be used to predict the *Rz*-index. To do this, we analyzed the coefficients of determination (*K*) of the dependence of *Rz*

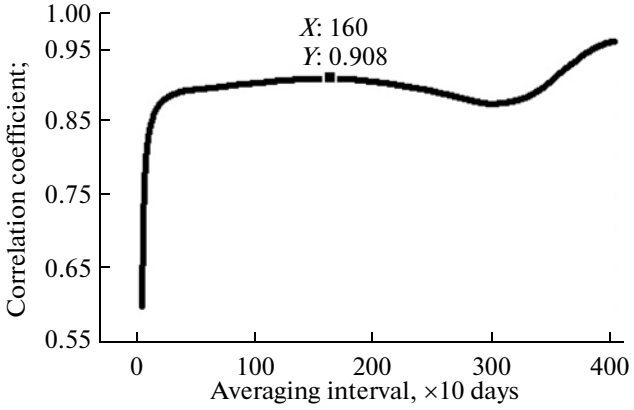

Fig. 7. Choice of the averaging interval for original data.

on the linear combination of $q(|pf|)$ and *ef* for different shifts of *ef* and the magnitude of *pf*. Figure 9 (left) shows the results of this study.

Figure 9 (right) shows only those linear dependences that have nonnegative coefficients at $q(|pf|)$ and *ef* (i.e., obtained without inversion, since we believe that the presence of a negative coefficient at $q(|pf|)$ and/or *ef* is unphysical).

It can be seen from Figure 9 (right) for the version without inversion that the maximum of the coefficient *K* (equal to 0.96) is obtained for the displacement *ef* = 0 years and for the displacement *pf* = 5.53 years.

Thus, to extend the horizon of prediction of the *Rz* index as a predictor, as follows from Fig. 9, one can use the time series of the magnitude of *pf* with a positive shift of $\Delta t = 5.5$ years. It is unreasonable to use the time series of *ef* since it has no positive shift.

Figure 10 shows the results of the linear prediction of variations in the polar field *pf* in the next cycle 24 (depicted as a magnitude). Now, to construct a prediction of the *Rz* index by variations of *pf*, we used the dependence of *Rz*(*pf*) on all available data and approximate this dependence by a parabola (Fig. 11).

In accordance with Fig. 11, we can obtain an analytical expression for the dependence *Rz*(|*pf*|):

$$Rz = 0.0063\, pf^2 + 0.1359\, pf + 20.7236.$$

Figure 12 shows the variations in the *Rz* index in cycle 24 predicted by the predicted variations of the

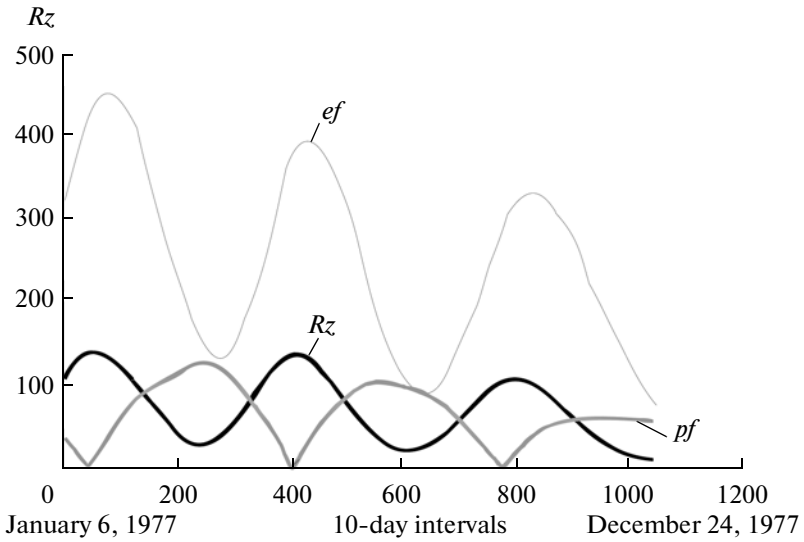

Fig. 8. Data on *Rz, ef*, and modulo *pf* averaged over 4.4-year intervals.

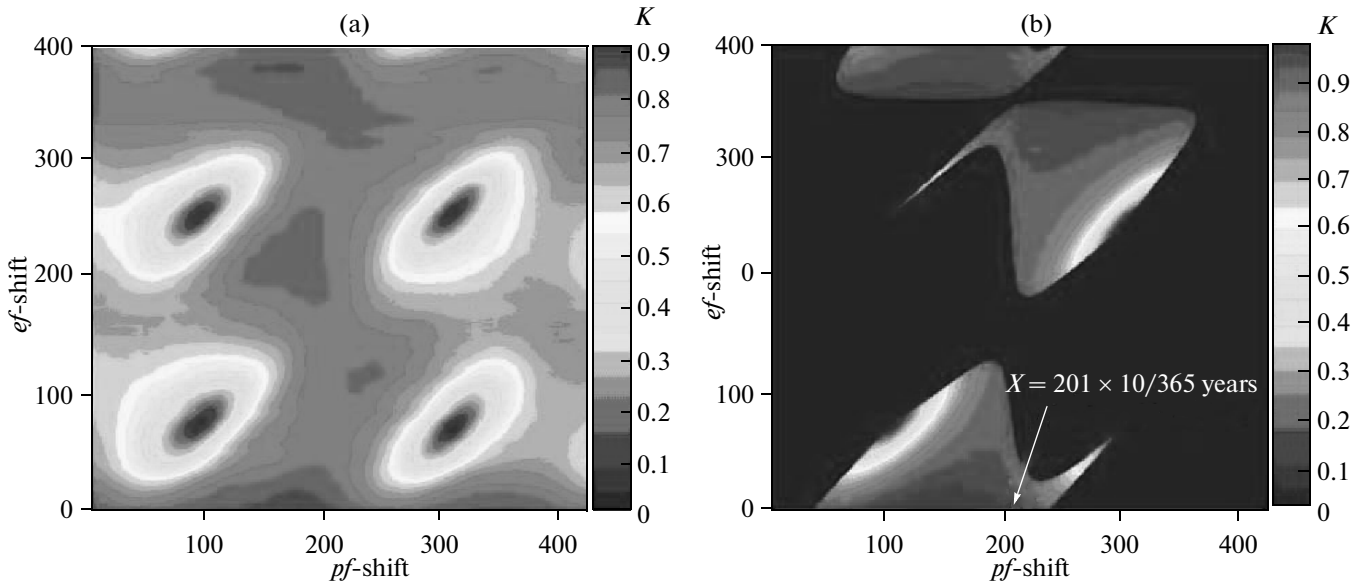

Fig. 9. Coefficient of determination (*K*) between *Rz* and forward displacement (necessary for the prediction) of the linear combination of averaged values of the time series for *ef* (96%) and modulo *pf* (6%); the "mosaic" pattern has a period of 10.3 years (left). The right panel shows the same except for the case of no inversion of the magnitude of *pf*.

magnitude of *pf* and the dependence between the magnitude of *pf* and the *Rz*-index (shown in Fig. 11).

As can be seen from Fig. 12, the parabolic approximation of the dependence of $Rz(|pf|)$ satisfactorily describes cycles 22 and 23. Within the framework of this model, the expected value of the maximum of *Rz* in cycle 24 was 50 and the time of the maximum was in April 2012. However, given the fact that initially the data was averaged over 4.4 years, the resulting maximum may be below the actual value. Therefore, one should stipulate that our predicted value of 50 units corresponds to average annual-mean smoothed values of *Rz*, equal to 60–70. This is close to that obtained by us in Section 2.2 (see Fig. 6) using a neural network approach.

4. DISCUSSION AND CONCLUSIONS

The onset of the minimum of solar cycle 23 was expected in 2006, but the decrease in solar activity

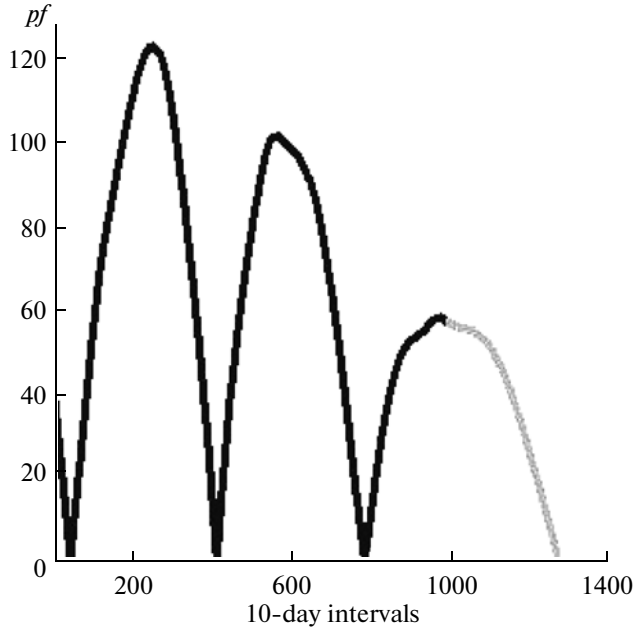

Fig. 10. Variations in the *pf* magnitude in cycles 22 and 23 together with the predicted values for cycle 24 (the gray curve).

lasted until early 2009. The protracted descending branch of cycle 23, which led to the fact that the cycle minimum was unusually prolonged, has long caused serious discussions in publications devoted to a comparative analysis of known historical cycles of solar activity as well as the current state of the characteristics of the interplanetary space (solar wind and the interplanetary magnetic field (IMF)) and the near-Earth space. In [Russell et al., 2010] it was shown that in late 2008 the periodic oscillations in the solar wind velocity observed earlier disappeared and the very magnitude of the velocity in late 2008 and 2009–2010 was no more than 300–350 km/s. Concurrently, a significant decrease in the intensity of energetic electrons in radiation belts was observed. The descending branch of cycle 23 involves a deep minimum of the IMF and the concentration of solar-wind protons with a continuing downward trend, which has never been previously observed from the very beginning of measurements of these parameters by space probes. A similar trend was also observed at high heliogeographic latitudes by the Ulyssis space probe [Smith and Balogh, 2008].

The protracted minimum of cycle 23, the situation in the near-Earth space corresponding to this cycle, and the anomalously low values of *Rz* at the maximum of cycle 24, as was predicted by us, are similar to the scenario of solar activity transition to the historical Dalton minimum in cycles 3–6 (Fig. 13). The extremely low solar activity in the Dalton minimum led to some cooling of the climate (for example, the River Thames froze and its ice cover was used for the 1814 London Fair).

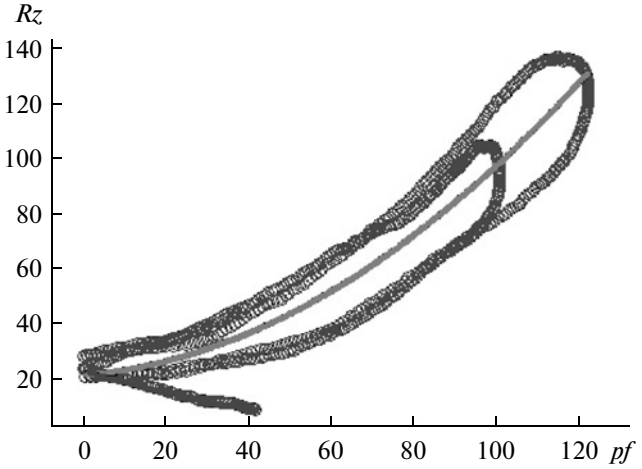

Fig. 11. Scatterplot of the joint distribution of the *pf* magnitude (shifted by 5.5 years) and the *Rz*-index. The red parabola indicates a nonlinear dependence between them.

In conclusion, our analysis of variations in the Wolf numbers *Rz* and attempts to predict solar cycle 24 by different methods in this paper showed the following:

(1) the proposed linear autoregressive (noniterative and iterative) methods yield large values of *Rz* (the amplitude of the maximum of cycle 24): 107 and 128, respectively. The resulting values are within the range predicted by the Third Official Solar Cycle Prediction Panel created by NASA, NOAA, and ISES for some approaches and models (120—160);

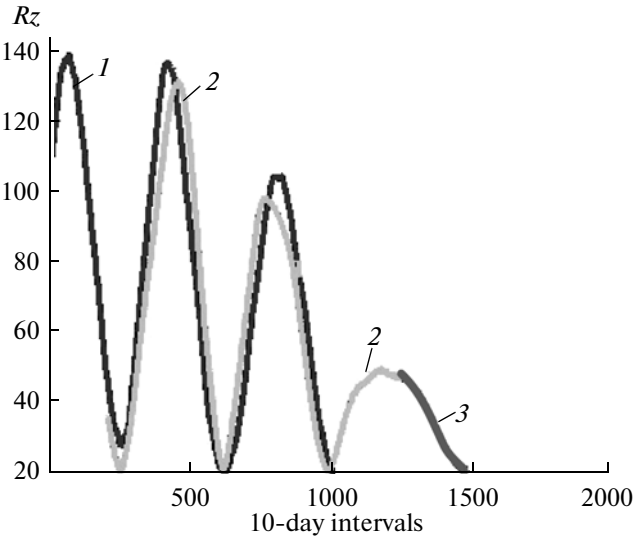

Fig. 12. Prediction values of *Rz* by the predicted polar field *pf* in cycle 24 taking into account the dependence of *Rz* on the *pf* magnitude shown in Fig. 11. (*1*) Original series, (*2*) approximation, and (*3*) prediction of solar activity.

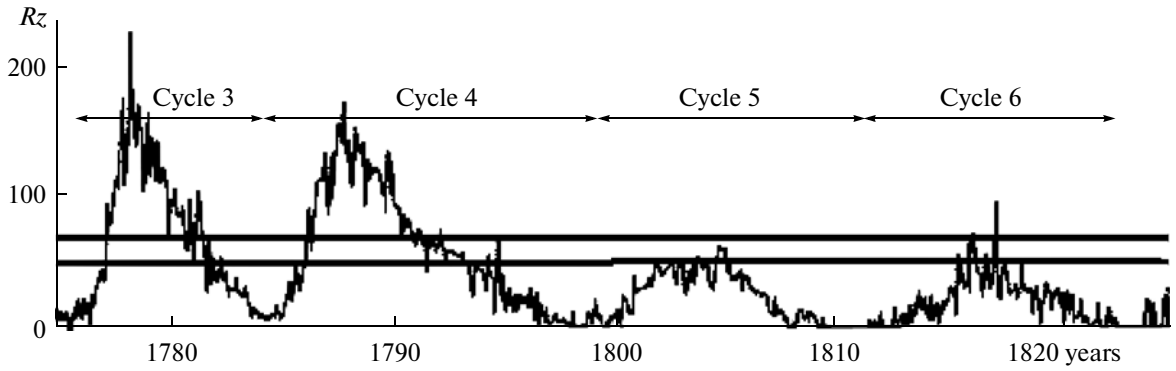

Fig. 13. Wolf numbers *Rz* during cycles 3–6 corresponding to the entry of solar activity into the Dalton minimum. The black bars denote the values of *Rz* for cycle 24 predicted by us.

(2) in contrast to other approaches, the nonlinear iterative method with a neural network allowed us to provide the best consistency between the predicted and actual values of *Rz* for both the unusually protracted cycle 23 and the initial phase of cycle 24. For the maximum amplitude of cycle 24, the predicted value is 70;

(3) the proposed precursor method allowed us to extend the horizon of the prediction of *Rz* by one cycle based on the dynamics of the solar polar magnetic field. This method suggests that the maximum of solar cycle 24 is expected to occur in April 2012 and its amplitude should be around 60—70. This is close to the value predicted by the neural network method.

ACKNOWLEDGMENTS

This work was supported by the Presidium of the Russian Academy of Sciences as part of the research project "Basic Research for Medicine." T.K. Breus is grateful to Lev Pustil'nik and Chris Russell for their useful discussions.

REFERENCES

Douglas Biesecker, 2008. http://www.swpc.noaa.gov/SolarCycle/SC24/

Duhau, S., An Early Prediction of Maximum Sunspot Number in Solar Cycle 24, *Sol. Phys.*, 2003, vol. 213, no. 1, pp. 203–213.

Fessant, P. and Lantos, P., Comparison of Neural Network and McNish and Lincoln Methods for the Prediction of the Smoothed Sunspot Index, *Sol. Phys.*, 1996, vol. 168, no. 2, pp. 423–433.

Feynman, I., Geomagnetic and Solar Wind Cycles, 1909–1975, *J. Geophys. Res.*, 1982, vol. 87, pp. 6153–6162.

Hathaway, D.H., Wilson, R.M., and Reichmann, E.J., A Synthesis of Solar Cycle Prediction Techniques, *J. Geophys. Res.*, 1999, vol. 104, p. 22375. doi 10.1029/1999JA900313

Kane, R.P., Did Predictions of the Maximum Sunspot Number for Solar Cycle 23 Come True, *Sol. Phys.*, 2001, vol. 202, no. 2, pp. 395–406.

Kane, R.P., Prediction of Solar Activity. Role of Long-Term Variations, *J. Geophys. Res.*, 2002, vol. 107, no. A7, pp. SSH3-1–SSH3-3.

Lantos, P. and Richard, O., On the Prediction of Maximum Amplitude for Solar Cycle Using Geomagnetic Precursors, *Sol. Phys.*, 1998, vol. 182, pp. 231–246.

Loskutov, A.N., Istomin, I.A., Kusanyan, K.M., and Kotlyarov, O.L., Testing and Forecasting the Time Series of the Solar Activity by Singular Spectrum Analysis, *Nonlinear Phenom. Complex Syst.*, 2001, vol. 4, no. 1, pp. 47–57.

Mahalanobis, P.C., On the Generalized Distance in Statistics, *Proceedings of the National Institute of Sciences of India*, 1936, vol. 2, no. 1, pp. 49–55.

Makarov, V.I. and Tlatov, A.G., The Large-Scale Solar Magnetic Field and 11-Year Activity Cycles, *Astron. Rep.,* 2000, vol. 44, no. 11, pp. 759–765.

McNish, A.G. and Lincoln, J.V., Prediction of Sunspot Numbers, *EOS Transact. AGU*, 1949, vol. 30, pp. 673–685.

McPherson, K.P., Conway, A.J., and Brown, J.C., Prediction of Solar and Geomagnetic Activity Data Using Neural Network, *J. Geophys. Res.*, 1995, vol. 100, no. A11, pp. 21735–21744.

Meyer, F. and De, A., Transfer Function Model for the Sunspot Number, *Sol. Phys.,* 2003, vol. 217, no. 2, pp. 349–366.

Obridko, V.N. and Kuklin, G.V., Solar Cycle Predictions based on Solar Cycle Phases, in *Sol.–Terr. Predic. Proc.,* Hruska, J., et al., Eds., 1994, vol. 2, pp. 273–298.

Obridko, V.N., Some Comments on the Problem of Solar Cycle Prediction, *Sol. Phys.*, 1995, vol. 156, pp. 179–190.

Ohl, A.I. and Ohl, G.I., A New Method of Very Long-Term Prediction of Solar Activity, in *Sol.–Terr. Predic. Proc.*, Donnely, R.F., Ed., Boulder, 1979, vol. 2, pp. 258–263.

Ozheredov, V.A., Breus, T.K., and Obridko, V.N., Singular Spectral Analysis in Solar–Terrestrial Physics, *Proceedings of the Russian–Bulgarian Conference, Sunny Beach, September Fundamental Space Research,* 2009, pp. 1–5.

Pesnell, W.D., Predictions of Solar Cycle 24, *Sol. Phys.*, 2008, vol. 252, pp. 209–220. doi 10.1007/s11207-008-9252-2

Petrovay, K., Solar Cycle Prediction, *Living Rev. Sol. Phys.*, 2010, vol. 7, pp. 6–59. http://www.livingreviews.org/lrsp-2010-6

Pyt'ev, Yu.P., *Metody analiza i interpretatsii eksperimenta* (Methods of Analysis and Interpretation of Experiments), Moscow: MGU, 1990.

Russell, C.T., Luhmann, J.G., and Jian, L.K., How Unprecedented a Solar Minimum, *Rev. Geophys.*, 2010, vol. 48, p. RG2004. doi 10.1029/2009RG000316

Schatten, K., Solar Activity Prediction. Timing Predictors and Cycle 24, *J. Geophys. Res.*, 2002, vol. 107, no. A11, pp. SSH15–SSH22.

Schatten, K., Solar Activity and the Solar Cycle, *Adv. Space Res.*, 2003, vol. 32, no. 4, pp. 451–460.

Smith, E.J. and Balogh, A., Decrease in Heliospheric Magnetic Flux in This Solar Minimum: Recent Ulysses Magnetic Field Observations, *Geophys. Res. Lett.*, 2008, vol. 35, p. L22103. doi 10.1029/2008GL035345

Svalgard, L., Cliver, E.W., and Kamide, Y., Sunspot Cycle 24: Smallest Cycle in 100 Years?, *Geophys. Res. Lett.*, 2005, vol. 32, p. L01104. doi 10.1029/2004GL021664

Wang, J.L., Gong, J.C., Liu, S.Q., et al., The Prediction of Maximum Amplitudes of Solar Cycles and the Maximum Amplitude of Solar Cycle 24, *Chin. J. Astron. Astrophys.*, 2002, vol. 2, pp. 557–562.